Available online at www.sciencedirect.com
ScienceDirect
Trans. Nonferrous Met. Soc. China 31(2021) 74−91
Transactions of Nonferrous Metals Society of China
www.tnmsc.cn

Wear behavior and dry sliding tribological properties of ultra-fine grained Al5083 alloy and boron carbide-reinforced Al5083-based composite at room and elevated temperatures

Matin SAESSI[1], Ali ALIZADEH[2], Alireza ABDOLLAHI[3]

1. Department of Composites, Malek-Ashtar University of Technology, Tehran, Iran;
2. Department of Materials and Manufacturing Processes, Malek-Ashtar University of Technology, Tehran, Iran;
3. Metallic Materials Research Center, Malek-Ashtar University of Technology, Tehran, Iran

Received 14 February 2020; accepted 7 September 2020

Abstract: Tribological behavior and wear mechanisms of mechanically milled Al5083 alloy and Al5083−5wt.%B_4C composite at room temperature and 200 °C were discussed. Results revealed that due to the oxidative wear at room temperature, a mechanically mixed layer (MML) was formed to protect the surface of the samples. Under 80 N of load at room temperature, the milled Al5083 and the Al5083−5wt.%B_4C samples showed evidence of abrasion with limited volume loss. In this case, the wear rates were 5.8×10^{-7} and 4.4×10^{-7} $mm^3/(m\cdot N)$, respectively. At 200 °C and under 80 N of applied load, severe wear occurred in the milled Al5083 sample, and wear rate reached 10.8×10^{-7} $mm^3/(m\cdot N)$ while the Al5083−5wt.%B_4C sample showed mild wear with local 3-body abrasion and the wear rate reached 5.3×10^{-7} $mm^3/(m\cdot N)$. Strengthening mechanisms such as dislocation pinning and the Hall−Petch theory, high hardness and the load transfer effect were crucial in determining the wear behavior of the Al5083−5wt.%B_4C composite. On the other hand, the milled Al5083 sample represented a relatively high wear rate at 200 °C, which seemed to be related to the local grain growth and a drop in its hardness.

Key words: tribological behavior; oxidative wear; mechanically mixed layer; wear rate; Hall−Petch theory

1 Introduction

Over the past few decades, aluminum matrix composites (AMCs) reinforced with hard ceramic particles and whiskers have been used in several industries such as aerospace and automotive for different purposes due to their superior properties such as low density, high specific strength, high room temperature corrosion resistance and low thermal expansion coefficient [1,2]. When it comes to high strength, ceramic-reinforced aluminum-based composites seem to be appropriate choices to work in different conditions. For instance, in the automobile engines, brake rotors and calipers, pistons and cylinder liners operate and work at temperatures up to $0.8T_m$ (melting point) of the aluminum alloy. Thus, investigating the high-temperature wear resistance of aluminum alloys reinforced by ceramic particles seems crucial. These studies are also important when in the case of die wear during hot forming procedures such as hot press and hot extrusion and the process of frictional welding involved in the joining of the composites [3,4]. Among a wide range of aluminum-based composites, boron carbide-reinforced Al5083-based composites are being used worldwide since they represent a high specific strength and are easy to be manufactured. The Al5083 alloy (series 5xxx) that contains about 4.4% magnesium, is a fine choice as the matrix of these composites since it represents lightweight, good

Corresponding author: Ali ALIZADEH; E-mail: alizadehh53@Gmail.com, A_Alizadeh@mut.ac.ir
DOI: 10.1016/S1003-6326(20)65479-6

ductility, weldability, corrosion resistance, and ease of manufacturing, and its density is a bit less than that of other conventional aluminum alloys (2.66 g/cm^3) [5]. It is widely used in the automotive industry and marine structures. Among the ceramic reinforcements, boron carbide has the closest density to Al5083 alloy (2.51 g/cm^3), hence, a homogeneous composite powder is made after the milling process with no agglomeration or separation [5,6]. During these years, Al−B_4C composites have been produced via different liquid and solid-state techniques such as stir casting and mechanical milling [5−8]. Many researchers have been working on these composites and other aluminum-based composites and they have studied their different features such as their physical and mechanical properties [5−8]. In our previous studies [5−7,9], several aspects of the Al−B_4C composites have been studied, nevertheless, almost no study has been done on comparing tribological behavior of Al5083−5wt.%B_4C composite with other samples especially at elevated temperatures. Tribological and wear behaviors of aluminum-based composites have always been a critical issue. For instance, IPEK [8] has stated that Al−B_4C composites are in the light and mild adhesive wear stage under different wear conditions at room temperature. SHOROWORDI et al [10] have reported that at room temperature, the coefficient of friction of the Al−B_4C samples decreases slightly at high contact pressures and the wear rate and friction coefficient of Al−B_4C are lower than those of Al−SiC. MAZAHERI et al [11] have reported that among different aluminum-based composites, Al−B_4C composite shows more wear resistance.

When studying the wear behavior of the aluminum-based composites at elevated temperatures, there are conflicting reports regarding the wear performance of aluminum alloys and aluminum-based composites. For instance, it has been mentioned that Al−Si−Mg (A356) alloys with and without SiC particles show mild to severe wear at about 0.4T_m of the aluminum due to the frictional heating under dry sliding conditions [12]. RAJARAM et al [13] have reported that oxidative wear is dominant in Al−Si alloys at elevated temperatures, which causes the high wear resistance of the material. MATHAVAN and PATNAIK [14] have indicated that by adding Ni, Cr and Si elements to the aluminum alloy, wear resistance increases significantly, and volume loss and wear rate decrease. GURCAN and BAKER [9] and KORAMAN et al [15] have reported that wear resistance in aluminum alloys and aluminum-based composites is directly related to the presence of reinforcements and the hardness of the samples. They have stated that the more the particle size of the reinforcement, the more the wear resistance, while SINGH and ALPAS [12] have reported that as the reinforcement particle size decreases, wear-resistant increases by pinning the dislocations in the sub-surface regions. TJONG et al [16] have reported that composites fabricated via the Ti−Al−B system show high wear rates since large TiB_2 agglomerates are present in the microstructure. In contrast, in situ aluminum-based composites fabricated via the TiO_2−Al−B system, show the minimum wear rate. The great wear performance of these composites is due to the formation of fine TiB_2 and Al_2O_3 particles, which are dispersed more uniformly in the aluminum matrix. KUMAR et al [17] reported an improvement in the wear performance of the Al−4Cu−TiB_2 composite by increasing the mass fraction of the reinforcement at all temperatures and loads. They have stated that the transition from mild to severe wear is strongly affected by the presence of the reinforcement particles. ZHANG and ALPAS [18,19] reported that the transition between mild and severe wear in aluminum-based composites is strongly dependent on the temperature, load, and sliding velocity. Eventually, since almost no report has been published concerning the study and comparing wear resistance and wear mechanisms of milled aluminum alloys and boron carbide-reinforced aluminum-based composites made via solid-state techniques at elevated temperatures, it seemed crucial to understand and to evaluate the wear performance and tribological behavior of these materials at low and high temperatures under different loads. In the present study, wear mechanisms and tribological behavior of ultra-fine grained Al5083 alloy and Al5083−5wt.%B_4C composite produced via mechanical milling at room temperature and 200 °C have been investigated and compared with un-milled Al5083 samples under the same conditions.

2 Experimental

Al5083−5wt.%B_4C and milled Al5083 samples were produced using commercial gas-atomized Al5083 powders with an average particle size of <100 μm and commercial boron carbide powders with an average size of <10 μm by mechanical milling, hot press, and hot extrusion procedures. Figure 1 indicates the SEM images and the cumulative particle size distribution analysis of the initial Al5083 and boron carbide composite of this study. The processing parameters and forming procedures were selected according to our previous research [20].

After the extrusion, three specimens with 5 mm in diameter and 10 mm in height were taken out from each sample. To study the mechanical milling and to confirm the steady-state occurrence, the Hall Funnel Method (ASTM — B417) was chosen. To measure the density and the porosity of the samples after the hot press step, the conventional Archimedes method was used according to the ASTM B962 — B417. Samples were kept in boiling water for over 5 h, then cooled down for over 24 h and finally weighed with a highly sensitive electronic balance (±0.0001 g). The porosity (P) of the samples was calculated based on Eq. (1):

$$P=(1-\frac{\rho_b}{\rho_T})\times 100\% \quad (1)$$

where ρ_b indicates the bulk density and ρ_T is the true density.

To investigate the wear performance of the samples, the pin-on-disk technique was chosen according to the ASTM G99 — 17. Tests were performed at room temperature (22−25 °C) and 200 °C under 20, 40 and 80 N of applied loads and the sliding distance of 1000 m with the linear speed of 50 cm/s using a standard “Ariana Modern San’at Wear Test Device” made in Iran. Samples were loaded vertically on the rotating AISI-O1 oil-hardened tool-steel disk with HRC 63 of hardness. Weights and volumetric measurements were done before and after the wear test (at least five times for each sample) and wear rates were calculated based on the volume loss by Eq. (2):

$$W=\frac{V}{DL} \quad (2)$$

where W is the wear rate ($mm^3/(m\cdot N)$), V is the volume loss (mm^3), D is the sliding distance (m) and L is the applied load (N). The hardness values of the samples at both room temperature and 200 °C were calculated according to the ASTM E92—17 based on the Vickers scale with 5 g of load and at least 3 to 5 indents. Worn surfaces and the morphology of the debris of the samples were examined using a Philips-XL30 scanning electron microscopy (SEM) device equipped with EDS spectroscopy. Friction coefficients (μ) and friction forces at room temperature and 200 °C are derived from Eq. (3):

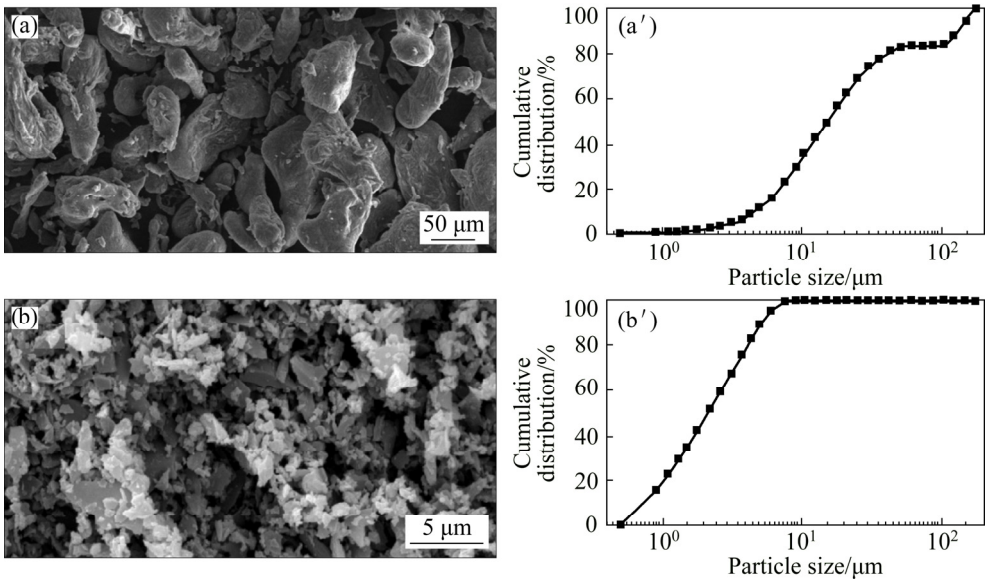

Fig. 1 SEM micrographs (a, b) and cumulative PSA analyses (a′, b′) of initial powders used in this study: (a, a′) Al5083; (b, b′) Boron carbide particles

$$\mu=\frac{F_f}{F_a} \quad (3)$$

where F_f indicates the friction load (N) and F_a indicates the normal applied load (N).

Table 1 shows a summary of the samples in this research with their processing conditions.

Table 1 Samples and their processing conditions in this study

Sample	Processing condition
Un-milled Al5083	Pure Al5083 powder→gas atomized→hot pressed and hot extruded
Milled Al5083	Pure Al5083→milled in an argon atmosphere for 36 h→hot pressed and hot extruded
Al5083−5wt.%B_4C	Al5083−5wt.%B_4C→milled in an argon atmosphere for 36 h→hot pressed and hot extruded

3 Results and discussion

3.1 Hardness and porosity measurements

Figure 2 indicates the apparent density curves vs milling time for the milled Al5083 and Al5083−5wt.%B_4C particles. As can be seen, after 36 h of milling, both samples showed the maximum density. Milling for more than 36 h did not change the apparent density of these two samples thus, it can be concluded that the steady-state is reached after 36 h of milling.

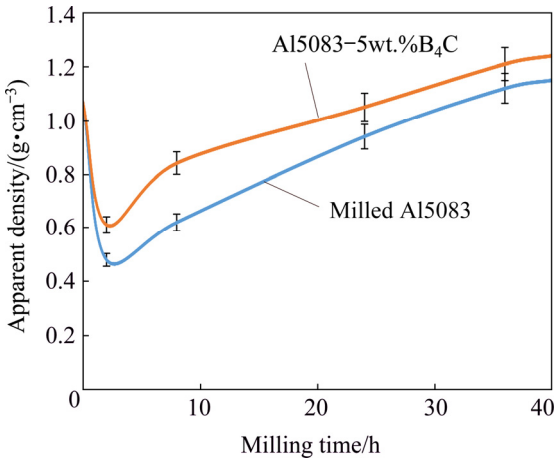

Fig. 2 Apparent density curves vs milling time of samples

Figure 3 indicates the SEM micrographs of the milled Al5083 and Al5083−5wt.%B_4C powder samples after milling for 36 h. Tiny equiaxed/spherical shaped particles of these samples compared to initial Al5083 powders (Fig. 1) confirm the steady-state occurrence of the mechanical milling.

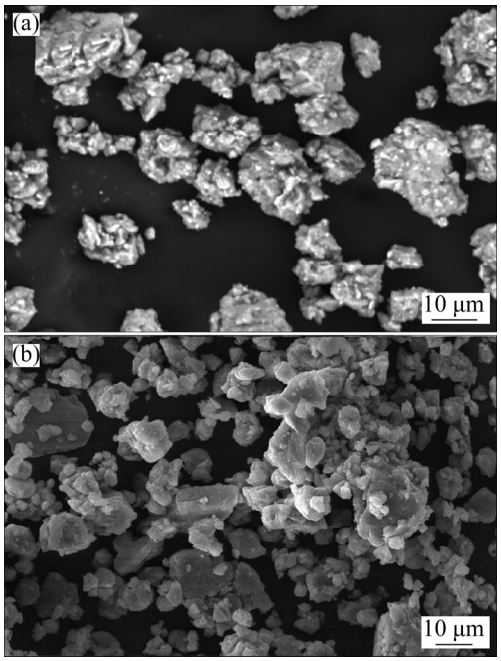

Fig. 3 SEM micrographs of milled powders after milling for 36 h: (a) Pure Al5083; (b) Al5083−5wt.%B_4C

It is well known that small spherical shaped powder particles lead to more apparent and bulk densities as powders can flow and slip on each other easily and fill in the holes [20−22].

Table 2 lists the hardness, ultimate tensile strength and porosity of the extruded samples. The milled Al5083 sample had more apparent density compared with the Al5083−5wt.%B_4C sample due to its uniform structure. In other words, due to the presence of the boron carbide reinforcement, the hardness of the powders of the Al5083−5wt.%B_4C sample increased, which led to less compressibility and more porosity. Moreover, the presence of some boron carbide particles in the microstructure hindered the perfect join between two Al−Al particles during the hot press and extrusion stages. This phenomenon led to more defects along the grain boundaries, which avoided perfect compression and thus, more porosity. Comparing Fig. 2 and Table 2 revealed that the more the apparent density of the powders, the less the porosity after the hot forming steps since under the pressure and shear stress, agglomerates are broken and tiny equiaxed particles can flow easily and roll on each other thus, they can move more easily and fill in the holes completely.

Table 2 Hardness, ultimate tensile stress and porosity of samples

Sample	Porosity/%	Hardness (HV)	UTS/MPa
Un-milled Al5083	0.2	88	212
Milled Al5083	0.4	228	343
Al5083−5wt.%B4C	0.7	357	509

On the other hand, the maximum tensile strength is related to the Al5083−5wt.%B_4C sample. This is due to the fine grain size of this sample and the strengthening mechanisms in aluminum-based composites. It is known that due to the Hall−Petch and Orowan strengthening mechanisms and the load-transfer effect, Al−B_4C composites represent high strengths [5,6,21]. This section has been explained with full details in our previous researches [5,20].

3.2 Microstructural characterization

Figure 4 shows the SEM micrographs of the samples after the hot press process. As can be seen in Fig. 4(a), grain boundaries are visible in the un-milled Al5083 sample while in the milled Al5083 and the Al5083−5wt.%B_4C samples (Figs. 4(b) and (c)), grain boundaries are not clearly visible. In fact, the milling process has led to an ultra-fine grained microstructure in both milled Al5083 and the Al5083−5wt.%B_4C samples since grains and grain boundaries cannot be easily recognized. Due to the severe plastic deformation and cold-welding and fracture occurrence during mechanical milling, grain refinement occurs remarkably which leads to a significant decrease in the grain size [5,20,21].

Figure 5 shows the TEM and FE-SEM images, EDS spectra, and XRD pattern of Al5083−5wt.%B_4C sample after hot press in which boron carbide and Al5083 particles can be easily identified.

The EDS spectra of this sample showed the presence of boron and carbon elements, which approved the presence of boron carbide particles in the Al5083 matrix. Moreover, the boron carbide peak is evident in the XRD pattern of this sample. On the other hand, boron carbide particles are embedded homogeneously in the Al5083 matrix.

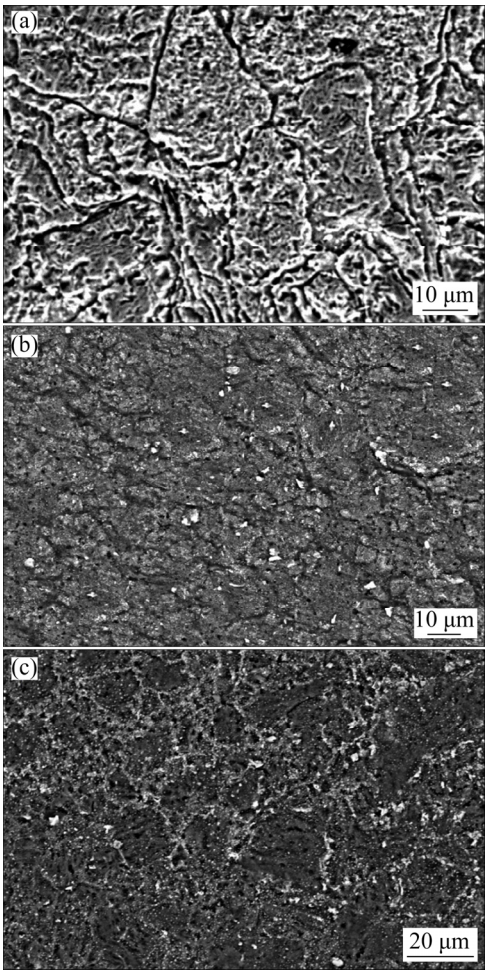

Fig. 4 SEM micrographs of samples after hot press process: (a) Un-milled Al5083; (b) Milled Al5083; (c) Al5083−5wt.%B_4C

Figure 6 shows the SEM and optical micrographs of the Al5083−5wt.%B_4C sample, parallel to the extrusion direction. It is expected that particles are elongated longitudinally along the extrusion direction; however, due to the severe dislocation pinning by the boron carbide reinforcement, particles have been elongated slightly along the extrusion direction. Furthermore, no pores, agglomerates or defects are visible, which indicates the effect of the hot extrusion process on the homogenous microstructure of the Al5083−5wt.%B_4C sample. It is known that due to the shear stress during the extrusion process, possible agglomerates are broken and a homogeneous microstructure with a fine dispersion of the reinforcement along the matrix is achieved. Moreover, the elongated grains fill in the defects and the reinforcements are embedded in the matrix [5,20].

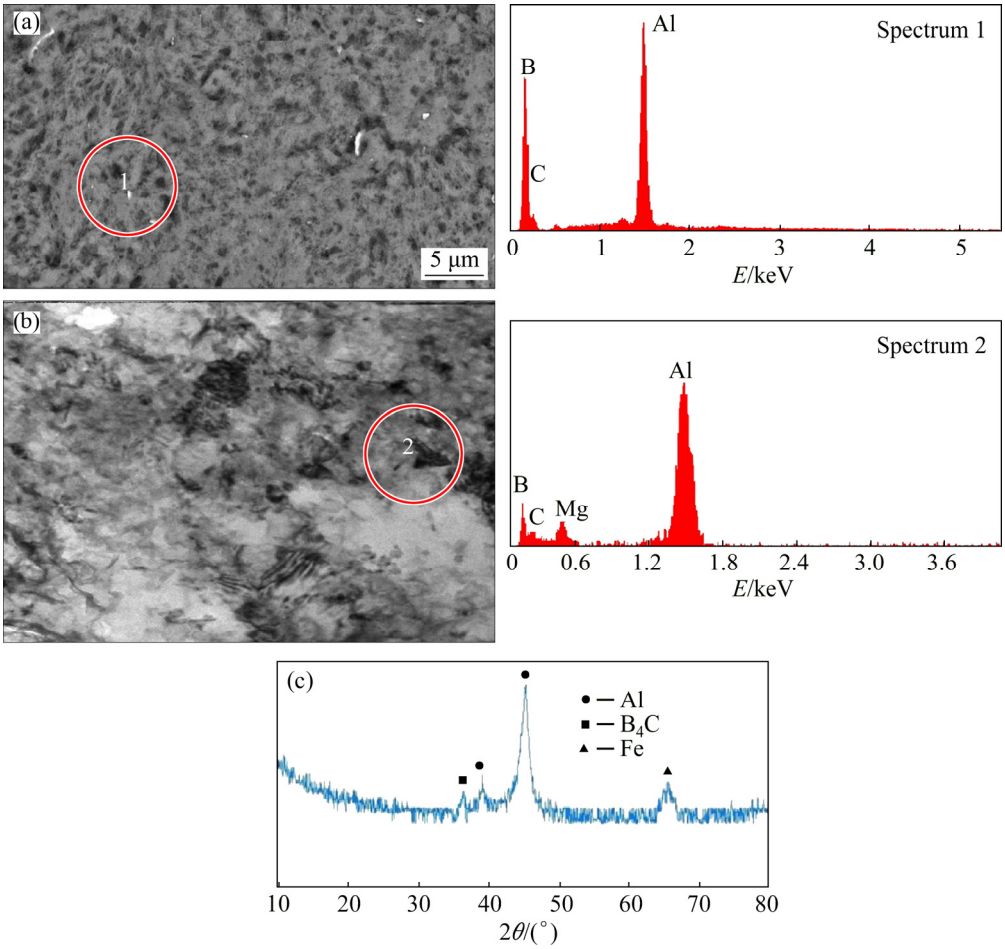

Fig. 5 FE-SEM (a) and TEM (b) micrographs and XRD pattern (c) of Al5083−5wt.%B_4C sample after hot press process and corresponding EDS analysis

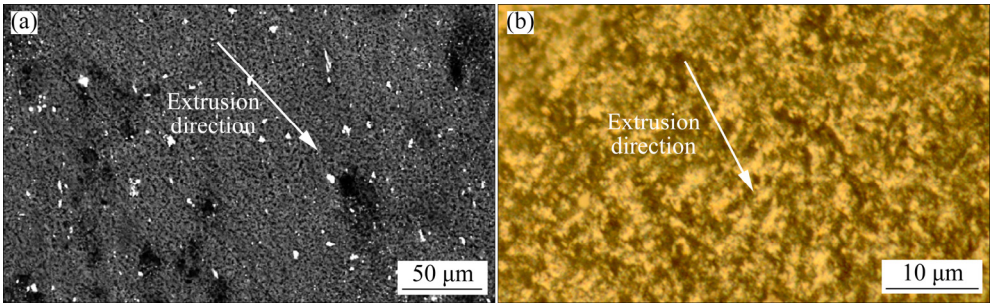

Fig. 6 SEM (a) and optical (b) micrographs of Al5083−5wt.%B_4C sample, parallel to extrusion direction

3.3 Wear rate analysis at room temperature and 200 °C

Figures 7 and 8 show the wear rates of the samples under 20, 40 and 80 N of applied loads at room temperature and 200 °C, respectively. It can be observed from Fig. 7 that at room temperature and under 80 N of applied load, the un-milled Al5083 sample showed the maximum wear rate of 12.9×10^{-7} $mm^3/(m\cdot N)$ while the Al5083−5wt.%B_4C sample showed the minimum wear rate of 4.4×10^{-7} $mm^3/(m\cdot N)$.

Similar results were gained at 200 °C in which the un-milled Al5083 sample showed the maximum wear rate of 14.7×10^{-7} $mm^3/(m\cdot N)$ while the Al5083−5wt.%B_4C sample showed the minimum wear rate of 5.3×10^{-7} $mm^3/(m\cdot N)$. It seemed that by increasing the applied load at both room temperature and 200 °C, the wear rate increased due to mass loss based on Eq. (2). In aluminum alloys, it is assumed that temperature rise enhances

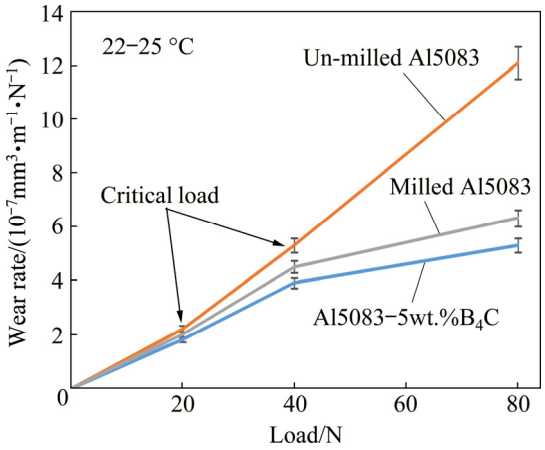

Fig. 7 Wear rates of samples under 20, 40 and 80 N of applied loads at room temperature

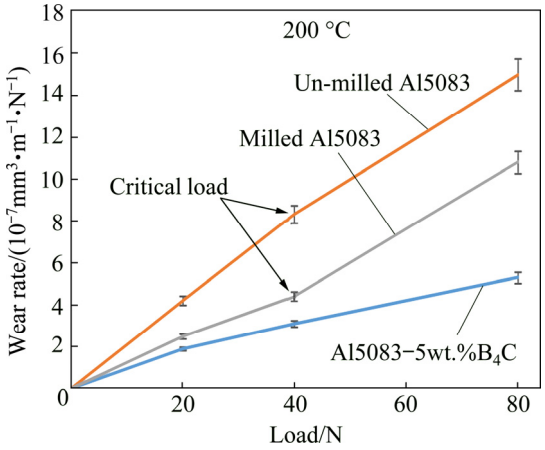

Fig. 8 Wear rates of samples under 20, 40 and 80 N of applied loads at 200 °C

the dislocation movements and dislocation slip and climb-glide happen, which leads to more plastic deformation [2,15]. Due to this plastic deformation at elevated temperatures and under high applied loads, failure and a drop in the strength and hardness of the sub-surface layers, occur remarkably at substrate layers. This leads to a significant increase in the wear rate [15]. On the other hand, it is known that the wear rate is inversely related to the hardness of the samples by Eq. (4), which is known as the Archard equation [15]:

$$W=\frac{KD}{H}L \tag{4}$$

where K is the wear constant, and H is the hardness of the samples.

It is expected that the wear rate of the samples is constant at certain temperatures and under certain loads. This was true for the wear rate of the samples under 20 N of the applied load. As shown in Fig. 7(a), samples at 22−25 °C showed similar wear rates under 40 N of the applied load. However, as the applied load increased to 80 N, the wear rate showed a remarkable difference. This was related to the change in the wear mechanism. This phenomenon seemed to be related to the effect of the temperature rise on the wear constant K and the wear mechanism. In other words, samples showed a deviation from the Archard equation. It seemed that at room temperature and 200 °C, the incline of the diagrams changed and deviation from the Archard equation occurred. Comparing the slopes of the curves in Figs. 7 and 8 indicated that under 20 N of applied load at room temperature, there was an increase for the un-milled Al5083 sample. This phenomenon can be explained by the transition between mild and severe wear. In other words, an increase in the slope of the wear rate−load curves indicates the transition from mild to severe wear. This can be considered as the critical load. Comparing Eq. (4) with the classic linear equation ($Y=AX+B$), it can be concluded that the slope (A), is equal to (KD/H), where K and D are constants at certain temperatures; hence, a change in the slope of the curves is attributed to a change in the hardness of the samples. In other words, a decrease in the slope indicates the material resistance to plastic deformation under applied load, which represents work hardening and other possible hardening mechanisms. Considering the wear rate−load curves of the un-milled Al5083 sample, it can be concluded that after the critical point, mild wear under 20 N changed to severer wear and more plastic deformation. Comparing the slopes of the curves for the milled Al5083 and the Al5083−5wt.%B_4C samples showed a slight decrease, which can be related to the faster formation of protective oxide layers and more dislocation pinning and lower dislocation movements, which caused no sensible plastic deformation. At 200 °C and under 20 N of applied load, the slope of the curve for the Al5083−5wt.%B_4C sample showed no significant change, which indicated no significant change in the wear mechanism. In other words, increasing the temperature to 200 °C did not have any significant effect on the dislocation movement in both surface and sub-surface layers in the Al5083−5wt.%B_4C sample due to the dominant strengthening

mechanism in aluminum-based composites reinforced with ceramic reinforcements. Remarkable dislocation pinning by the boron carbide reinforcements leads to almost no plastic deformation under different loads in sub-surface layers. Comparing Figs. 7 and 8 with Figs. 4 and 6 suggested that due to the fine grain size of the milled Al5083 and Al5083−5wt.%B_4C samples, they represented more hardness due to the Hall−Petch theory and thus, more wear resistance. Considering the Hall−Petch and Archard theories, it can be concluded that strengthening mechanisms, such as fine grain size, high dislocation pinning, and high hardness of the samples, play a crucial role in determining the wear rate and the wear resistance of the Al5083−B_4C composites.

3.4 Wear mechanisms and tribological behavior at room temperature

Table 3 lists the coefficients of friction of un-milled, milled and Al5083−5wt.%B_4C samples derived from wear tests under different applied loads at room temperature. The maximum coefficient of friction is for un-milled Al5083 while the minimum is related to the Al5083−5wt.%B_4C sample. Comparing the coefficients of friction at different loads revealed that as the applied load increased, the coefficient of friction decreased. To explain this issue, two major factors must be considered: the rate of oxide layer formation and the rate of oxide layer removal. It is expected that increasing the applied load from 20 to 80 N leads to a local increase in the coefficient of friction at the initial stage of wear procedure; however, the increase in the friction level leads to an increase in the surface temperature as well.

Table 3 Coefficients of friction of samples derived from wear tests under different applied loads at room temperature (22−25 °C)

Sample	Applied force/N	Coefficient of friction
Un-milled Al5083	20	1.41
	40	0.98
	80	0.78
Milled Al5083	20	1.35
	40	0.88
	80	0.65
Al5083−5wt.%B_4C	20	1.28
	40	0.83
	80	0.59

Temperature rise enhances the formation of oxide layers such as aluminum and iron oxides. These oxide layers protect the surface from being worn and avoid the adhesion between pin (sample) and disk surfaces. In other words, these oxide layers act as barriers or lubricants at the pin/disk interface and avoid plastic deformation on the wear surface. This phenomenon leads to surface protection and a decrease in the coefficient of friction. Moreover, as the hardness of the Al5083−5wt.%B_4C sample was rather high, friction led to local absorption of iron from the disk. Iron absorption increases the hardness of the surface in aluminum alloys by the formation of aluminum and iron oxides (which is called the MML). This oxide layer acts as a lubricant and prevents direct contact between the pin surface and the disk thus, it reduces the coefficient of friction in the Al5083−5wt.%B_4C sample. This is consistent with the results reported by some other researchers about the formation of the oxide protective layer [15,16,21].

Figure 9 shows the SEM images and EDS spectra of the worn surfaces of the Un-milled and milled Al5083 and Al5083−5wt.%B_4C samples under 20 N of applied load at room temperature. Comparing Figs. 9(a), (b) and (c), revealed that since the applied load was rather low, no significant plastic deformation occurred, which confirmed mild abrasive wear in all the samples. EDS spectra of these samples indicated the presence of oxygen, which can be related to the oxidative wear and the formation of the oxide protection layer during the wear test. Comparing the amount of oxygen in all samples confirms similar wear performances of these samples. The friction force between the pin surface and the disk during the wear test leads to an increase in the surface temperature, which enhances the oxidative wear. The presence of these oxide layers prevents surface damage by acting as lubricants. Figure 9(d) shows the wear debris of the Al5083−5wt.%B_4C sample. Tiny equiaxed particles prove the mild and abrasive wear mechanism of this sample. EDS spectrum of the surface of the Al5083−5wt.%B_4C sample (Fig. 9(c′)) indicated the presence of iron and more amount of oxygen, which proved more absorption of iron and more oxide formation.

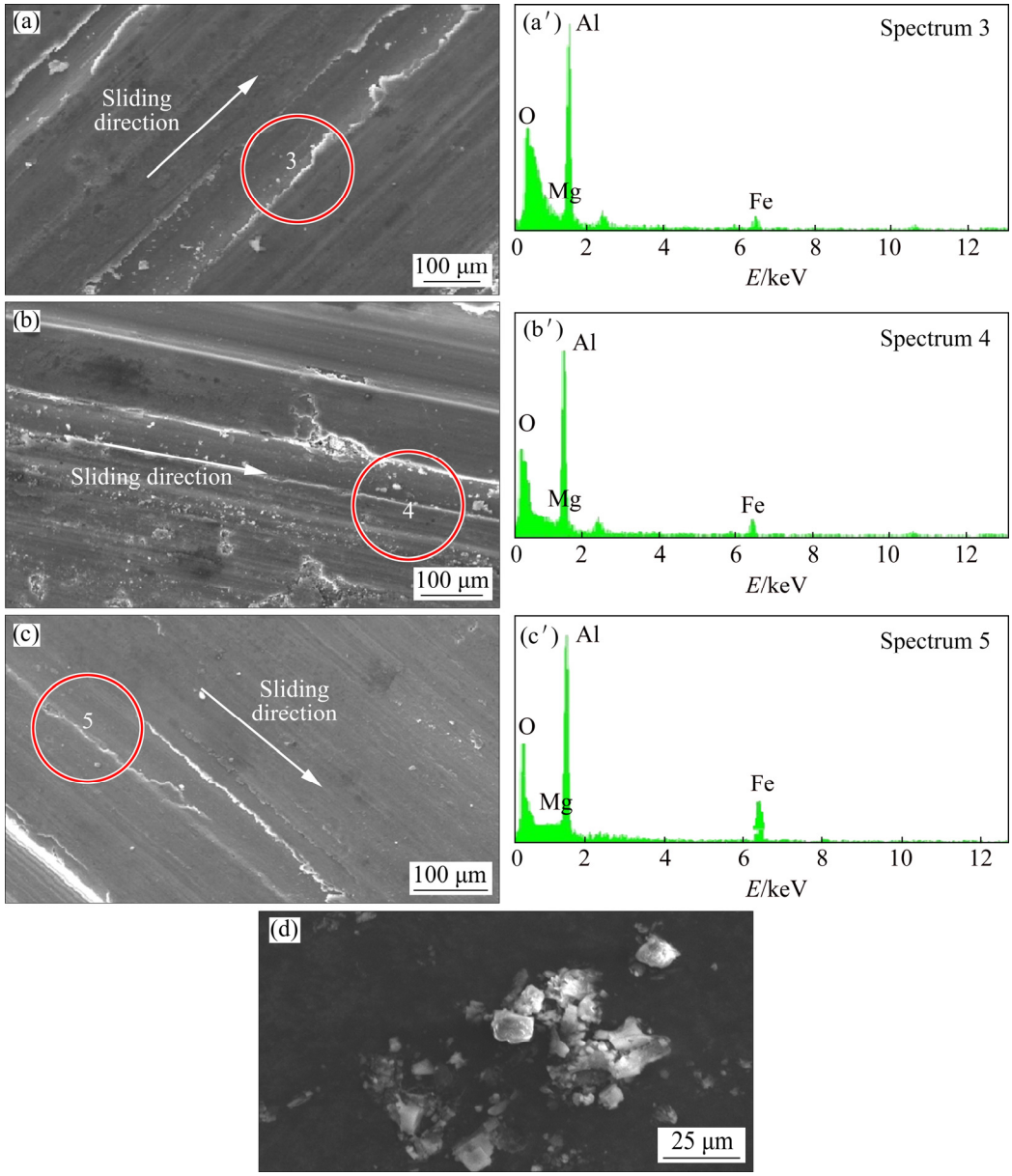

Fig. 9 SEM micrographs (a, b, c) and corresponding EDS analyses (a′, b′, c′) of worn surfaces and debris of samples under 20 N of load at room temperature: (a, a′) Un-milled Al5083; (b, b′) Milled Al5083; (c, c′) Al5083−5wt.%B_4C; (d) Wear debris of Al5083−5wt.%B_4C

Figure 10 shows the SEM images of worn surfaces of the Un-milled and milled Al5083 and Al5083−5wt.%B_4C samples under 40 N of the applied load at room temperature. Comparing Figs. 10(a), (b) and (c) revealed that as the applied load reached 40 N, significant plastic deformation occurred in the Un-milled Al5083 sample, and wear mechanism changed while in the other two, no severe plastic deformation occurred. It can be said that as the Un-milled Al5083 sample had the minimum hardness, the pin cut deeply into the surface and a remarkable plastic deformation occurred on the surface, which caused surface damage under the applied load. EDS spectra of these samples indicated the presence of oxygen, which can be related to the presence of the oxide protective layers. However, comparing the amount of oxygen in Figs. 10(a′), (b′) and (c′), confirms a decrease in oxygen amount of Un-milled Al5083 sample under 40 N of the applied load. It seemed that as the applied load reached 40 N, oxidative layers were damaged locally; however, plastic deformation in the sub-surface layers, may avoid the oxide layer to be removed. This phenomenon

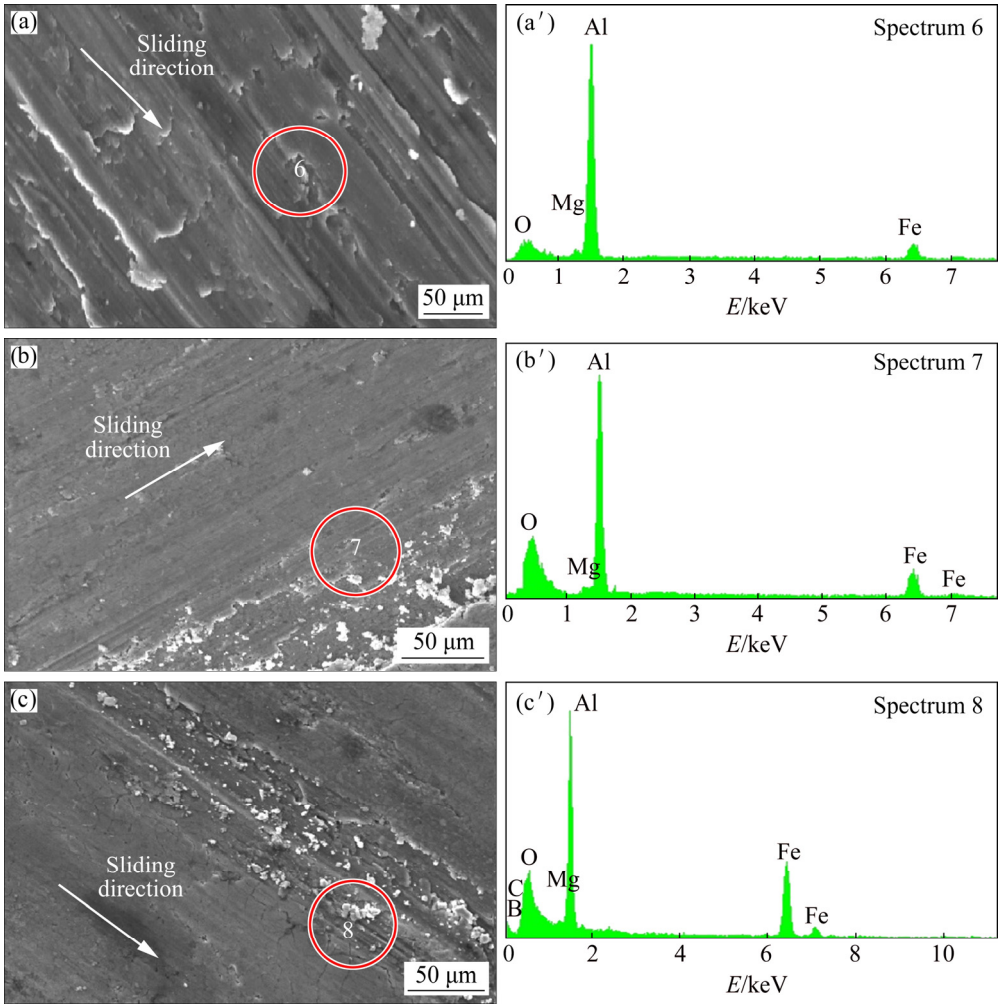

Fig. 10 SEM micrographs (a, b, c) of worn surfaces of samples under 40 N of applied load at room temperature and corresponding EDS analyses (a′, b′, c′): (a, a′) Un-milled Al5083; (b, b′) Milled Al5083; (c, c′) Al5083−5wt.%B_4C

resulted in a decrease in oxygen with more damage in some areas of the pin surface. On the other hand, comparing Figs. 9 and 10 revealed that as the applied load reached 40 N, extensive plastic deformation occurred in Un-milled Al5083 while in milled Al5083 and Al5083−5wt.%B_4C samples, no significant change on the worn surfaces occurred. This phenomenon confirmed similar wear mechanisms under 20 and 40 N of applied loads in milled Al5083 and Al5083−5wt.%B_4C samples. Comparing Fig. 10 with Table 3 confirmed the formation of the oxide protective layer on the surface of the milled Al5083 and the Al5083−5wt.%B_4C samples and the low coefficient of friction in these samples.

Worn surfaces and the EDS spectra of the Un-milled and milled Al5083 and Al5083−5wt.%B_4C samples under 80 N of load are illustrated in Fig. 11. Comparing Figs. 11(a), (b) and (c), indicated significant plastic deformation with surface damage in the Un-milled Al5083 sample in comparison with the milled Al5083 and Al5083−5wt.%B_4C samples, which suggested the adhesion mechanism. Moreover, comparing Figs. 11(b) and (c) revealed that the presence of boron carbide particles enhanced wear resistance of Al5083−5wt.%B_4C sample even under 80 N of load since no severe surface damage was evident in this sample. However, there was evidence of some cavities. This seemed to be due to the defects of this sample. Comparing Fig. 11 with Table 2 revealed that since this sample had a few defects, cracks could be initiated along with the defects in sub-surface regions under 80 N of load and thus, material removal from some parts of the surface. Nevertheless, due to the maximum hardness of

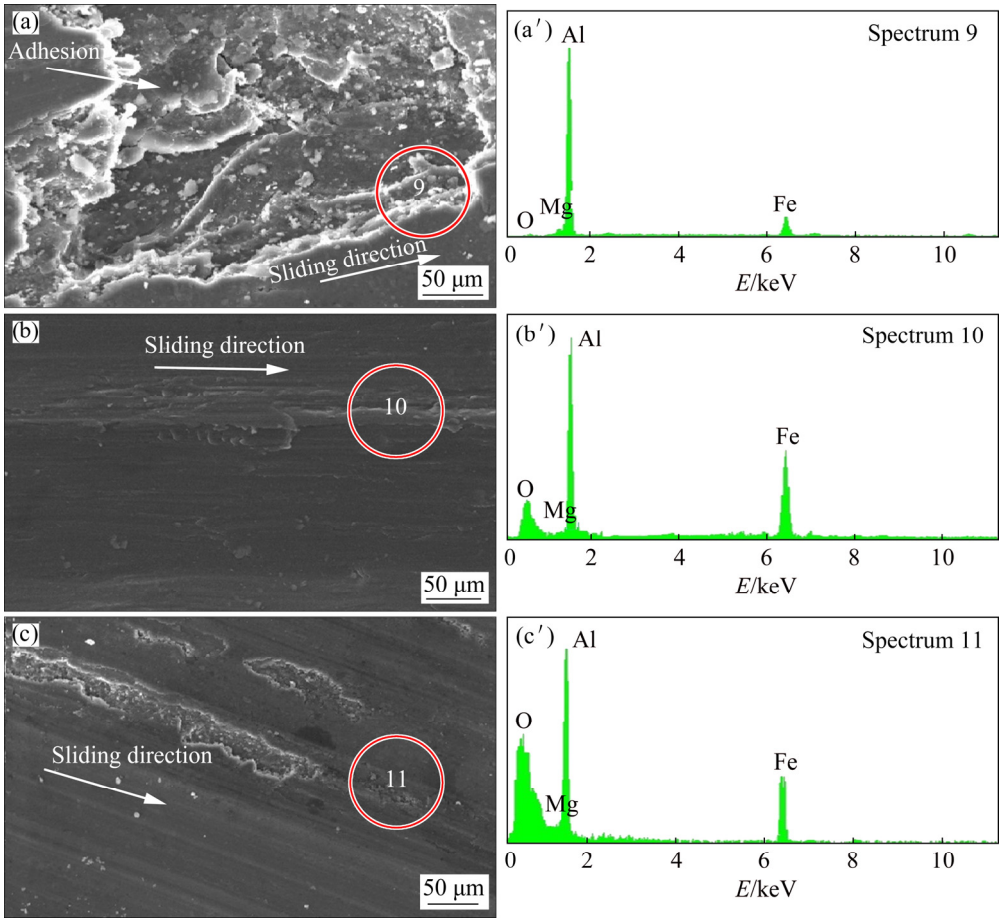

Fig. 11 SEM micrographs (a, b, c) and corresponding EDS analyses (a′, b′, c′) of worn surfaces of samples under 80 N of applied load at room temperature: (a, a′) Un-milled Al5083; (b, b′) Milled Al5083; (c, c′) Al5083−5wt.%B_4C

Al5083−5wt.%B_4C sample and the load transfer effect, the wear resistance of Al5083−5wt.%B_4C sample is more than that of milled Al5083 sample. On the other hand, comparing the EDS spectra of the milled Al5083 and Al5083−5wt.%B_4C sample reveals absorption by the surface. It can be said that due to the maximum hardness of the Al5083−5wt.%B_4C sample, abrasion in this sample led to more iron absorption from the disk. Comparing the amount of oxygen on the surface of the samples indicated that by increasing the applied load from 40 to 80 N, the amount of oxygen in the un-milled Al5083 sample became very limited. It seemed that due to the minimum hardness of this sample, the oxide protection layer was damaged and removed from the surface.

Figure 12 shows the wear debris of the Un-milled Al5083 sample under 80 N of the applied load at room temperature with its EDS spectrum. Irregular and randomly shaped particles with large thicknesses indicate severe wear. Furthermore, the

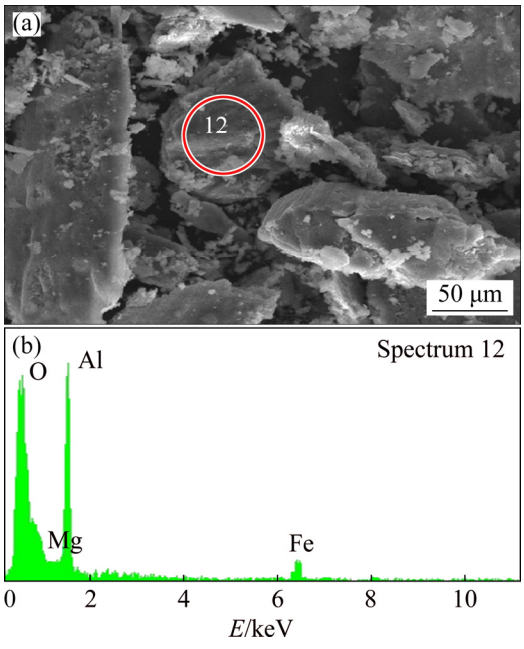

Fig. 12 Wear debris of un-milled Al5083 sample under 80 N of applied load at room temperature (a) and corresponding EDS spectrum (b)

EDS spectrum of the debris indicates considerable amount of oxygen, which confirms the presence of oxide particles in debris. These particles seem to be due to the fracture occurrence of the oxide layer during wear test and the oxide layer removal. In other words, as the applied load reached 80 N, intensive fracture occurred in the protective oxide layer, which led to the direct contact between the pin surface and the disk and the adhesion occurrence. The adhesion between the pin surface and the disk led to crack growth in sub-surface regions, which led to a fracture of the surface protective layer and significant material loss.

Eventually, it can be concluded that at room temperature and under different loads, milled Al5083 and Al5083−5wt.%B_4C samples exhibited mild abrasion while the Un-milled Al5083 sample showed mild to severe wear as the load increased. These phenomena indicate the effect of hardness and grain size on the wear resistance of ultra-fine grained aluminum bulks and aluminum-based composites. Moreover, wear resistance showed a remarkable improvement by adding 5 wt.% of boron carbide, which can be due to the strengthening mechanisms and the load-transfer effect. Some researchers have reported similar results about the wear behavior of Al-based composites at room temperature [8,10,18,19,21].

3.5 Wear mechanism and tribological behavior at 200 °C

Table 4 lists the hardness and coefficients of friction of the samples at 200 °C. It is evident that the maximum coefficient of friction is for Un-milled Al5083 while the minimum is related to the Al5083−5wt.%B_4C sample. Furthermore, comparing Tables 3 and 4 indicated that the coefficient of friction increased by increasing the temperature. It is said that aluminum alloys show a decrease in their hardness at temperatures higher than 150 °C [4,6] as a result, it seemed that high temperature during wear tests caused the hardness of the surface of the samples to decrease. Hence, more contact between the pin surface and the disk occurred, which led to an increase in the coefficient of friction. On the other hand, comparing coefficients of friction at 200 °C suggested that as the load increased, the coefficient of friction decreased. This phenomenon might be related to the quick formation of oxide protective layers on the surface at this temperature. Temperature rise enhances the formation of oxides, which act as lubricants and lead to surface protection.

Table 4 Hardness and coefficients of friction of samples derived from wear tests under different applied loads at 200 °C

Sample	Hardness (HV)	Applied force/N	Coefficient of friction
Un-milled Al5083	78	20	1.55
		40	0.87
		80	0.58
Milled Al5083	210	20	1.42
		40	0.80
		80	0.55
Al5083−5wt.%B4C	374	20	1.32
		40	0.78
		80	0.48

Figure 13 shows the SEM images of the worn surfaces and EDS spectra of the un-milled and milled Al5083 and Al5083−5wt.%B_4C samples under 20 N of applied load at 200 °C.

By comparing the images, one can understand that at 200 °C, the un-milled Al5083 sample (Fig. 13(a)) showed evidence of severe plastic deformation followed by local delamination while in the milled Al5083 and Al5083−5wt.%B_4C samples (Figs. 13(b) and (c)), mild abrasion occurred. In other words, under 20 N of applied load, Al5083−5wt.%B_4C showed no sensible plastic deformation, which indicated mild wear and no surface adhesion.

Figure 14 shows the SEM images and EDS spectra of the worn surfaces of the milled Al5083 sample under 40 and 80 N of applied loads at 200 °C. Evidence of mild wear and abrasion was clearly visible from Fig. 14(a). Moreover, it seemed that due to the high load and more contact between the pin and the disk and due to the brittleness of this sample, crack propagation occurred in some sub-surface regions and the MML layer could not stand on the surface of the milled sample under 80 N of the load. In fact, sub-surface layers could not support the MML layer. This led to a local material loss in some areas on the surface. Comparing the worn surfaces of the milled sample (Figs. 14(a) and (b)) suggested that by making the applied load double from 40 to 80 N, more

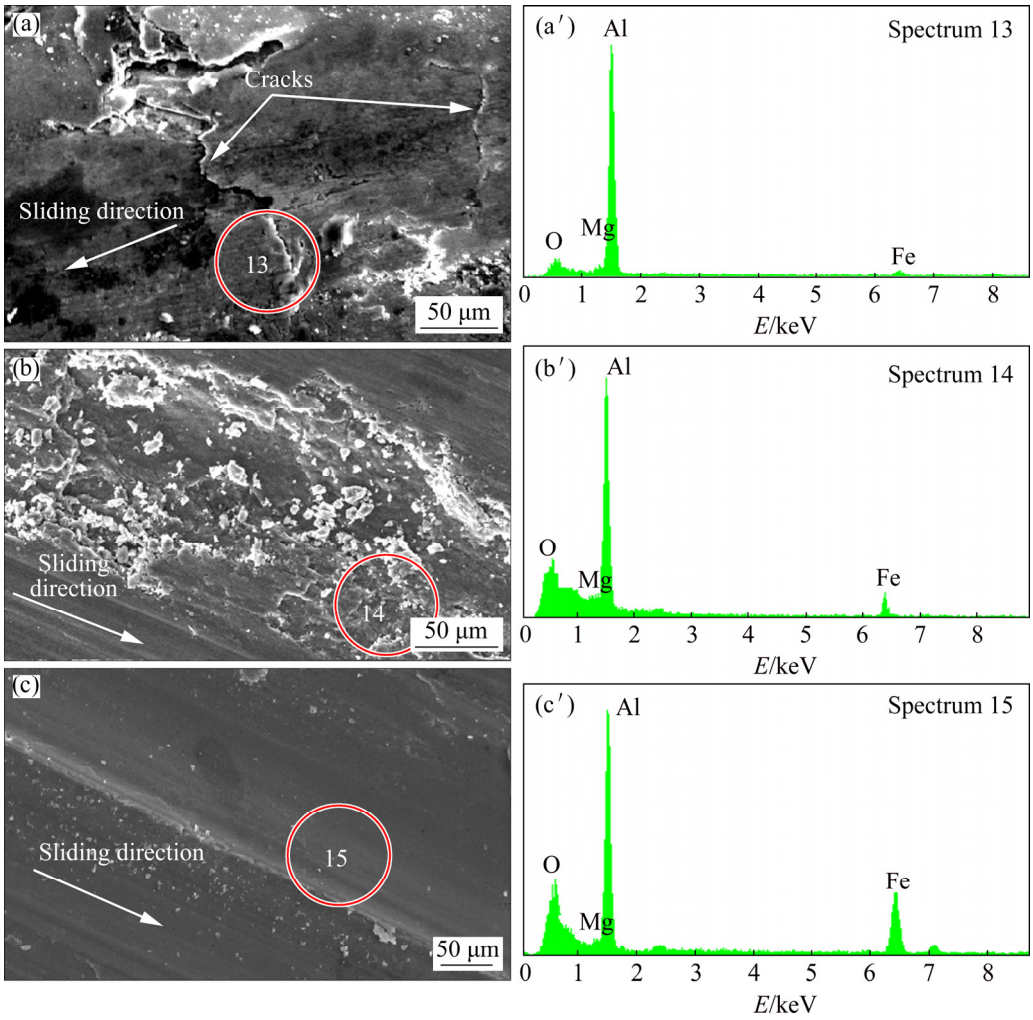

Fig. 13 SEM micrographs (a, b, c) of worn surfaces of samples under 20 N of applied load at 200 °C and corresponding EDS spectra (a′, b′, c′): (a, a′) Un-milled Al5083; (b, b′) Milled Al5083; (c, c′) Al5083−5wt.%B_4C

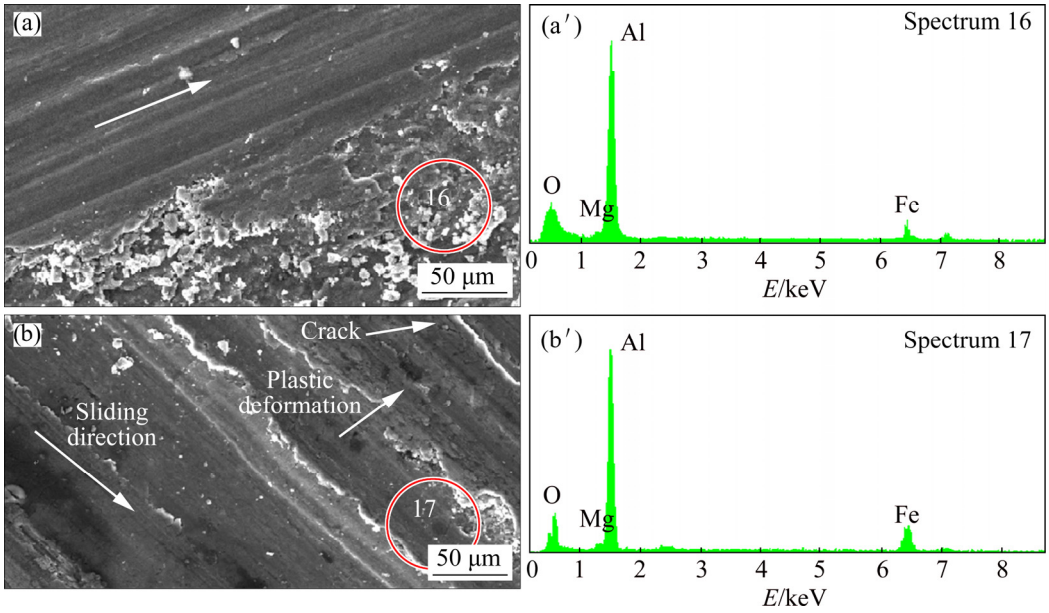

Fig. 14 SEM micrographs (a, b) of worn surfaces of milled Al5083 sample under different loads at 200 °C and corresponding EDS spectra (a′, b′): (a, a′) 40 N; (b, b′) 80 N

adhesion led to more local plastic deformation occurrence and an increase in the wear rate and a transition from mild to severe wear. The increase in the wear rate of this sample seemed to be related to local plastic deformation and further failure of mechanically mixed layers. As mentioned earlier, the formation of oxide layers is enhanced by the temperature rise. As a result, oxide layers are formed more quickly under 80 N of load and at 200 °C in the milled Al5083 sample. However, due to the high applied load, the rate of oxide layer removal was rather high. Fractured oxide particles were acted as abrasives, which led to a significant increase in the wear rate. In other words, at 200 °C, the wear mechanism changed from abrasion to abrasion−local delamination.

Figure 15 shows the SEM images of the worn surfaces of the Al5083−5wt.%B_4C sample under 40 and 80 N of applied load at 200 °C [23]. It is clear that in both samples, abrasive wear occurred extensively; however, increasing the applied load from 40 to 80 N led to deeper cavities and significant material loss in some areas of the surface. By increasing the applied load, the load-transfer mechanism occurs more rapidly and the load is transferred to boron carbide particles, which holds the wear resistance. However, high-applied load and the presence of boron carbide particles with fractured oxide particles caused local 3-body abrasion and surface damage. SEM images and EDS spectra of the Al5083−5wt.%B_4C sample at 80 N of load proved the existence of oxides and iron along with boron and carbon, which confirmed the presence of boron carbide and oxides and thus, 3-body abrasion occurrence. Transverse cracks, which are visible along the sliding direction (Fig. 15(b)), might have been initiated in work-hardened layers and sub-surface regions due to the lack of plastic deformation. As the cracks got interconnected, fracture occurred in oxide layers, which caused local 3-body abrasion. These phenomena led to a local increase in the wear rate of the Al5083−5wt.%B_4C sample at elevated temperatures under 80 N of the applied load.

Figure 16 shows a schematic diagram of the 3-body abrasion mechanism. As shown in Fig. 16, the presence of reinforcement particles with the fractured oxide particles from the MML acts as abrasives and enhances 3-body abrasion. This causes more iron absorption, material loss, surface damage and high wear rates. Comparing Figs. 15 with 16 confirmed the local 3-body abrasion occurrence in the Al5083−5wt.%B_4C sample. Comparing Figs. 14 with 15 revealed that despite 3-body abrasion occurrence in the Al5083−5wt.%B_4C sample, wear resistance was more than the milled Al5083 sample. This is due to the local dislocation movements and plastic deformation of the milled Al5083 sample under 80 N of the load compared with obstructed dislocation movements

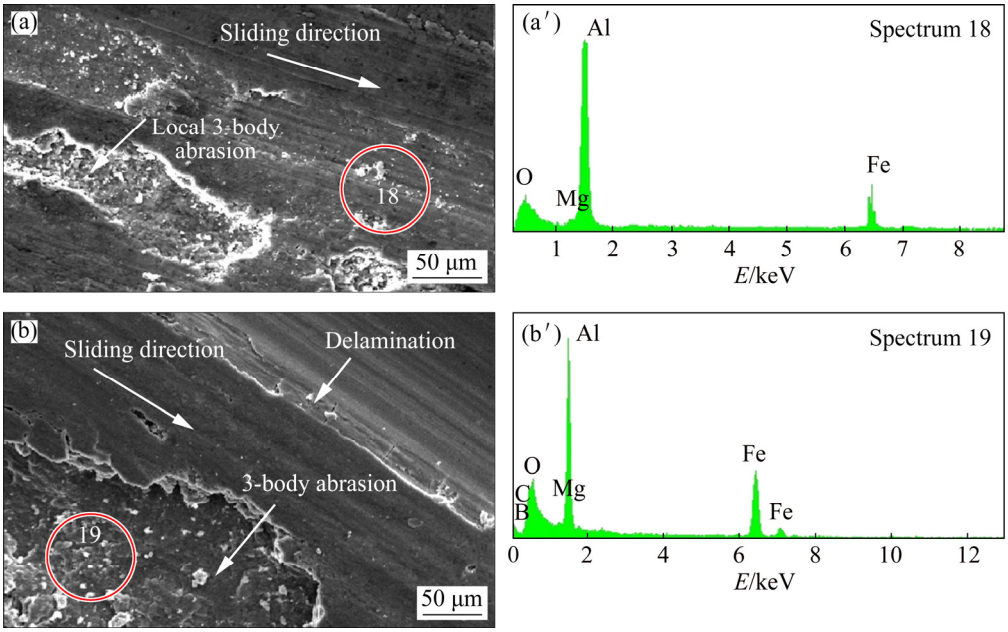

Fig. 15 SEM micrographs (a, b) of worn surfaces of Al5083−5wt.%B_4C sample under different loads at 200 °C and corresponding EDS spectra (a′, b′) [23]: (a, a′) 40 N; (b, b′) 80 N

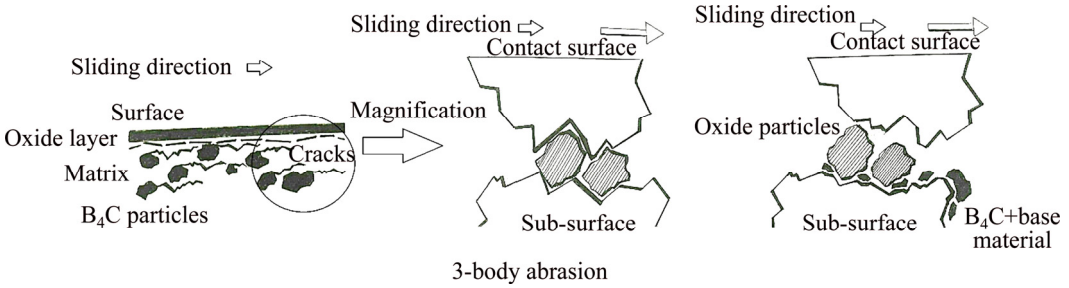

Fig. 16 Schematic diagram indicating 3-body abrasion mechanism

in the Al5083−5wt.%B_4C sample. Besides, by comparing Figs. 14 and 15 with Tables 2 and 4, it can be said that the hardness of the milled Al5083 sample slightly decreased at 200 °C while almost no loss occurred in the hardness of the Al5083−5wt.%B_4C sample. Thus, due to the Archard theory, the more wear rate and the less wear resistance existed for the milled Al5083 sample at 200 °C under 80 N of the applied load.

Besides, these results seemed inconsistent with the results reported by SINGH and ALPAS [12] about the wear resistance of the aluminum-based composites at elevated temperatures. They have stated that at elevated temperatures, mild wear changes to severe wear due to the frictional heating under dry sliding conditions while this phenomenon did not seem to happen in our study. It is assumed that due to the mechanical milling procedure and the fine dispersion of the boron carbide reinforcement particles in the Al5083 matrix, severe dislocation pinning occurred and thus, no plastic deformation occurred to enhance the transition between mild to severe wear. Besides, since boron carbide particles are embedded firmly in the Al5083 matrix during mechanical milling, high temperature and load could not weaken the interface between the boron carbide and the matrix, hence, wear resistance of this sample did not change remarkably at 200 °C.

Figure 17 shows the sub-surface regions of the un-milled Al5083 and Al5083−5wt.%B_4C samples after the wear test under 80 N of applied load at 200 °C. As can be seen, it is evident that in the un-milled Al5083 sample, severe plastic deformation occurred (Fig. 17(a)) while in the Al5083−5wt.%B_4C sample, no remarkable change in the sub-surface regions occurred (Fig. 17(b)). In other words, adhesion wear and severe plastic deformation led to a remarkable change in the

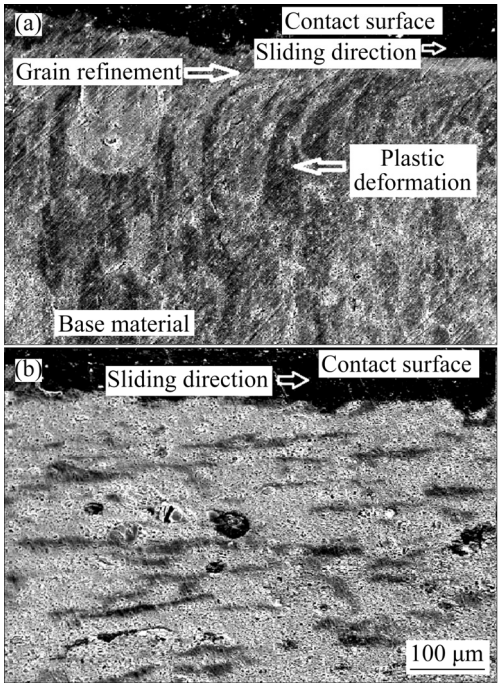

Fig. 17 SEM micrographs of sub-surface regions of samples under 80 N of applied load at 200 °C: (a) Un-milled Al5083; (b) Al5083−5wt.%B_4C

formation of sub-surface layers near the surface at about 400 μm from the contact surface. Due to the maximum hardness of the Al5083−5wt.%B_4C sample and significant dislocation pinning, no deformation in sub-surface regions occurred. On the other hand, at the depth of about 200 μm from the contact surface, grain refinement is evident due to the high temperature and ultra-fine grains are visible. It is said that at temperatures between 150 and 350 °C, recrystallization, grain refinement and local grain growth occur [4]. Due to the high temperature during wear test and the high load (high friction force) on the contact surface of this sample, the temperature seemed to be above 200 °C which led to grain refinement and the formation of fine aluminum grains in this area. This is consistent

with the results reported by RICE et al [24] about the deformation zones in the sub-surface regions of aluminum samples. They have stated that applying loads during the wear process leads to plastic deformation in the sub-surface regions along the sliding direction [24].

Figure 18 represents a schematic diagram of the deformation zones in the sub-surface regions in aluminum samples [23,24]. Comparing Fig. 17 with Fig. 18 confirms the presence of the deformation zones in the sub-surface regions of the un-milled Al5083 sample during the wear test due to its relatively low hardness and significant plastic deformation.

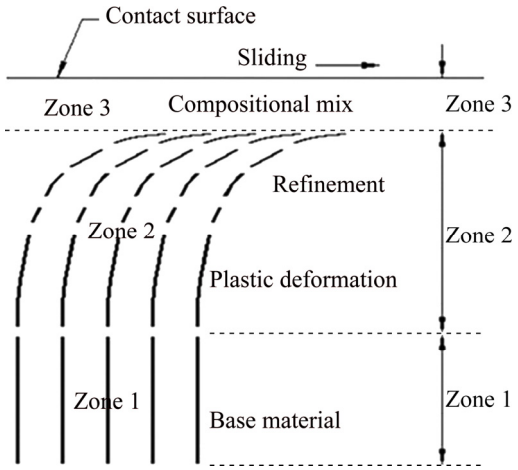

Fig. 18 Schematic diagram of deformation zones in sub-surface regions in aluminum-based samples [23,24]

Figure 19 shows the optical images of the subsurface regions of the un-milled and milled Al5083 samples after the wear test under 80 N of applied load at 200 °C. Comparing Figs. 18 and 19 revealed that local grain growth and plastic deformation occurred in the milled Al5083 sample. It seemed that grain growth occurrence was due to the high temperature and the instability of the microstructure of this sample. In fact, applied tension and temperature at the same time led to local dislocation movements, climb and glide occurrence, and the reformation of dislocations. Comparing Figs. 17 and 19 indicated that due to the local grain growth of this sample and considering the Hall−Petch theory, hardness decreased, and thus, wear resistance decreased in the milled Al5083 sample.

Eventually, it can be concluded that the wear performance of Al5083−5wt.%B_4C under high

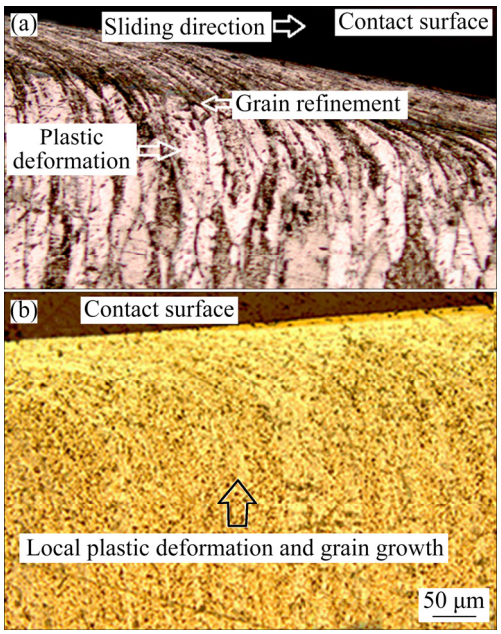

Fig. 19 Optical micrographs of sub-surface regions of samples under 80 N of applied load at 200 °C: (a) Un-milled Al5083; (b) Milled Al5083

applied loads and at elevated temperatures is directly related to the strengthening mechanisms, the rate of oxide layer formation and the rate of oxide layer removal. Due to the higher rate of formation and removal of oxide layers at high temperatures under high applied loads, fractured oxide particles act as abrasives and enhance local 3-body abrasion, which leads to an increase in the wear rate. Nevertheless, due to the dislocation pinning in this sample, transition between mild to severe wear does not happen. This phenomenon does not happen in the milled Al5083 sample since no reinforcement or dislocation pinning occurs. Thus, wear performance of this sample is determined by the local grain growth and the Hall−Petch theory.

4 Conclusions

(1) Under different loads, Al5083−5wt.%B_4C sample showed lower wear rates compared with mechanically milled ultra-fine grained Al5083 samples and similar wear rates at both room temperature and 200 °C achieved.

(2) At 200 °C and under 80 N of applied load, severe adhesion occurred for the un-milled Al5083 sample while for the ultra-fine grained Al5083, delamination was the dominant wear mechanism

and in Al5083−5wt.%B_4C sample, a combination of abrasion and local 3-body abrasion occurred due to the presence of reinforcements and the load-transfer effect.

(3) At room temperature, increasing the load from 40 to 80 N did not affect the wear mechanism and abrasion is the dominant mechanism in Al5083−5wt.%B_4C sample. This is related to local surface temperature increase and faster formation of the protective oxide layer.

(4) Increasing the temperature to 200 °C did not affect the strength and hardness of the sub-surface layers in Al5083−5wt.%B_4C since severe dislocation pinning occurred due to the presence of boron carbide particles. No grain growth occurred due to the pinning of the grain boundaries and abrasion was the dominant wear mechanism due to the formation of the oxide protective layer and the hardness of this sample.

(5) As the load increased, the coefficient of friction decreased due to the formation of oxide layers, which were acted as lubricants.

Acknowledgments

Authors would like to appreciate the former chief of Faculty of Materials & Manufacturing Processes of the Malek-Ashtar University of Technology, Professor EHSANI and the chief of the Composite Department, Dr. POURHOSSEINI along with the Razi and Kimiazi SEM labs and mechanical properties and SEM labs of Iran University of Science and Technology. Furthermore, the authors would like to thank Professor REZAEI, Ms. HAMIDI, and Ms. DAYYANI, Mr. SA'ADAT, and Mr. ATAEI from Iran University of Science and Technology. Special thanks to Mrs. KESHAVARZ, Ms. HAMEDANIZADEH, Ms. SHABANI, Ms. SHOJAEI and Mr. GANDOMKAR for their help and support.

References

[1] MIRACLE D B. Metal matrix composites–from science to technological significance [J]. Composites Science and Technology, 2005, 65: 2526−2540.

[2] ALIZADEH A, MALEKI M, ABDOLLAHI A. Preparation of super-high-strength nanostructured B_4C reinforced Al−2Cu aluminum alloy matrix composites by mechanical milling and hot press method: Microstructural, mechanical, and tribological characterization [J]. Advanced Powder Technology, 2017, 28: 3274−3287.

[3] KHADEMIAN M, ALIZADEH A, ABDOLLAHI A. Fabrication and characterization of hot rolled and hot extruded boron carbide (B_4C) reinforced A356 aluminum alloy matrix composites produced by stir casting method [J]. Transactions of the Indian Institute of Metals, 2017, 70: 1635−1646.

[4] SINGH J, ALPAS A T. Elevated temperature wear of Al6061 and Al6061−20%Al_2O_3 [J]. Scripta Metallurgica et Materialia, 1995, 32(7): 1099−1105.

[5] ALIZADEH A, ABDOLLAHI A, RADFAR M J. Processing, characterization, room temperature mechanical properties and fracture behavior of hot extruded multi-scale B_4C reinforced 5083 aluminum alloy based composites [J]. Transactions of Nonferrous Metals Society of China, 2017, 27: 1233−1247.

[6] SAESSI M, ALIZADEH A, ABDOLLAHI A, EHSANI N. Room temperature wear performance and mechanical properties of hot extruded ultrafine-grained Al5083−5wt%B_4C-Al2024 tri-modal composites [J]. Materials Research Express, 2019, 6: 096549.

[7] SAESSI M, ALIZADEH A. Comparative studies on microstructural evolution, mechanical properties and room temperature dry sliding tribological behavior of nano-crystalline Al5083 alloy produced by the cryobox technique [J]. Materials Research Express, 2019, 6: 0965a2.

[8] IPEK R. Adhesive wear behavior of B_4C and SiC reinforced 4147 Al matrix composites (Al/B_4C−Al/SiC) [J]. Journal of Materials Processing Technology, 2005, 162: 71−75.

[9] GURCAN A B, BAKER T N. Wear behavior of AA6061 aluminum alloy and its composites [J]. Wear, 1995, 188: 185−191.

[10] SHOROWORDI K M, HASEEB A S M A, CELIS J P. Tribo-surface characteristics of Al−B_4C and Al−SiC composites worn under different contact pressures [J]. Wear, 2006, 261: 634−641.

[11] MAZAHERI Y, MERATIAN M, EMADI R, NAJARIAN A R. Comparison of microstructural and mechanical properties of Al−TiC, Al−B_4C, and Al−TiC−B_4C composites prepared by casting techniques [J]. Materials Science and Engineering A, 2013, 560: 278−287.

[12] SINGH J, ALPAS A T. High-temperature wear and deformation processes in metal matrix composites [J]. Metallurgical and Materials Transactions A, 1996, 27: 3135−3148.

[13] RAJARAM G, KUMARAN S, RAO T S. High temperature tensile and wear behavior of aluminum-silicon alloy [J]. Materials Science and Engineering A, 2010, 528: 247−253.

[14] MATHAVAN J J, PATNAIK A. Analysis of wear properties of aluminum-based journal bearing alloys with and without lubrication [J]. IOP Conference Series: Materials Science and Engineering, 2016 149: 012052.

[15] KORAMAN E, BAYDUGAN M, SAYILGAN S, KALKANH A. Dry sliding wear behavior of Al−Fe−Si−V alloys at elevated temperatures [J]. Wear, 2015, 322: 101−107.

[16] TJONG S C, WU S Q, ZHU H G. Wear the behavior of in situ $TiB_2{\cdot}Al_2O_3$/Al and $TiB_2{\cdot}Al_2O_3$/Al−Cu composites [J]. Composites Science and Technology, 1999, 59: 1341−1347.

[17] KUMAR S, SARMA V S, MURTY B S. High temperature

wears behavior of Al−4Cu−TiB_2 in situ composites [J]. Wear, 2010, 268: 1266−1274.

[18] ZHANG J, ALPAS A T. Wear regimes and transitions in Al_2O_3 particulate-reinforced aluminum alloys [J]. Materials Science and Engineering A, 1993, 161: 273−284.

[19] ZHANG J, ALPAS A T. The transition between mild and severe wear in aluminum alloys [J]. Acta Materialia, 1997, 45: 513−528.

[20] SAESSI M, ALIZADEH A, ABDOLLAHI A. On the analysis of fracture mechanisms and mechanical behavior of AA5083-based tri-modal composites reinforced with 5 wt.% B_4C and toughened by AA5083 and AA2024 coarse grain phases [J]. Advanced Powder Technology, 2019, 30: 1754−1764.

[21] ABDOLLAHI A, ALIZADEH A, BAHARVANDI H R. Dry sliding tribological behavior and mechanical properties of Al2024−5wt.%B_4C nanocomposite produced by mechanical milling and hot extrusion [J]. Materials & Design, 2014, 55: 471−481.

[22] FOGAGNOLO J B, VELASO F, ROBERT M H, TORRALBA J M. Effect of mechanical alloying on the morphology, microstructure and properties of aluminium matrix composite powders [J]. Materials Science and Engineering A, 2003, 342: 131−143.

[23] SAESSI M, ALIZADEH A, ABDOLLAHI A. On the analysis of high-temperature mechanical properties and dry sliding tribological behavior of ultra-fine grained boron carbide-reinforced Al5083-based trimodal composites [J]. Journal of Bio- and Tribo-Corrosion, 2020, 6(3): 1−20.

[24] RICE S L, NOWOTNY H, WAYNE S F. A survey of the development of subsurface zones in the wear of materials [J]. In Key Engineering Materials, 1989, 33: 77−100.

超细晶 Al5083 合金和碳化硼增强 Al5083 基复合材料的室温和高温干滑动摩擦磨损行为

Matin SAESSI[1], Ali ALIZADEH[2], Alireza ABDOLLAHI[3]

1. Department of Composites, Malek-Ashtar University of Technology, Tehran, Iran;
2. Department of Materials and Manufacturing Processes, Malek-Ashtar University of Technology, Tehran, Iran;
3. Metallic Materials Research Center, Malek-Ashtar University of Technology, Tehran, Iran

摘　要：讨论机械球磨 Al5083 合金和 Al5083−5wt.%B_4C 复合材料在室温和 200 °C 下的摩擦行为和磨损机制。结果表明，由于常温下的氧化磨损，形成可保护试样表面的机械混合层。在室温和 80 N 载荷下，Al5083 和 Al5083−5wt.%B_4C 球磨样品有磨损迹象，但体积磨损量有限，磨损率分别为 5.8×10^{-7} 和 4.4×10^{-7} $mm^3/(m\cdot N)$。在 200 °C 和 80 N 载荷下，球磨 Al5083 样品磨损严重，磨损率达 10.8×10^{-7} $mm^3/(m\cdot N)$；Al5083−5wt.%B_4C 样品的磨损较轻，局部出现三体磨损，磨损率为 5.3×10^{-7} $mm^3/(m\cdot N)$。位错钉扎和 Hall−Petch 理论等强化机制、高硬度和载荷传递效应是决定 Al5083−5wt.%B_4C 复合材料磨损行为的关键因素。另一方面，球磨 Al5083 样品在 200 °C 下磨损率较高可能与其局部晶粒长大和硬度下降有关。

关键词：摩擦行为；氧化磨损；机械混合层；磨损率；Hall−Petch 理论

(Edited by Xiang-qun LI)